ICARUS 75, 113–126 (1988)

Enceladus: Implications of Its Unusual Photometric Properties

BONNIE J. BURATTI

Jet Propulsion Laboratory, California Institute of Technology, 4800 Oak Grove Drive, Pasadena, California 91109

Received July 2, 1985; revised December 7, 1987

We have investigated the photometric properties of Enceladus up to phase angles of 43°, using Voyager 1 and 2 images. Among the satellite's unusual photometric characteristics are its very high geometric albedo (1.0 ± 0.1 near 0.47 μ), which extends down to at least 0.34 μ, and the uniformity of albedos, colors, and scattering properties over the geologically varied surface. Although some albedo variations of up to 15% occur in low resolution Voyager 1 images, the albedos of the four major geological units imaged in the Voyager 2 near-encounter sequence differ by 1–2% or less, even though the ages of these units probably differ by at least a factor of 10 (3.8 billion years to a few hundred million years). The lack of correlation of spectrophotometric properties with terrain type suggests that the optical characteristics of Enceladus are determined by a recently deposited ubiquitous surface layer, possibly originating in Saturn's E-ring. The high geometric albedo implies that the surface layer is remarkably free of opaque material and is much more backscattering than is common for natural or laboratory frost layers on Earth. The unique phase and photometric functions of Enceladus can be explained by the high degree of multiple scattering in its surface. The existing observations suggest that the textural characteristics of Enceladus' regolith are similar to those of other icy Saturnian satellites.

I. INTRODUCTION

The Saturnian satellite Enceladus is a remarkable object. With a visual geometric albedo close to unity, it is by far the most reflective known solid body in the Solar System (Franz and Millis 1975, Cruikshank 1979, Smith *et al.* 1982, Buratti and Veverka 1984). High resolution Voyager images depict geologic activity which occurred less than 1 billion years ago on about half of its surface (Smith *et al.* 1982). Based on assumptions concerning the flux of impacting bodies, Plescia and Boyce (1983) have suggested that heavily cratered portions of the remaining area are more than 3.8 billion years old. Because the orbital position of Enceladus coincides with the position of maximum density of the tenuous, extended E-ring (Baum *et al.* 1981), active geologic processing on Enceladus has been invoked as the source mechanism for E-ring particles. The flatness of the satellite's spectrum into the ultraviolet (Buratti 1984) further points toward the existence of fresh ice on its surface.

A final element of the puzzling aspects of this satellite is that substantial surficial albedo variations were detected as early as 1914 by Lowell and Slipher (see Franz and Millis 1975). They found that the satellite was 0.3 mag brighter at western elongation than eastern elongation. Franz and Millis (1975) measured a total amplitude of 0.4 mag and confirmed a maximum in brightness at the same position, which corresponds to the trailing side of Enceladus. The other inner icy Saturnian satellites, Dione, Rhea, and Tethys, all have brighter leading sides; Mimas does not have a well-defined orbital light curve (Noland *et al.* 1974, Franz and Millis 1975, Buratti and Veverka 1984).

In this paper, we investigate the color

0019-1035/88 $3.00

TABLE I

LIST OF IMAGES

Image FDS No.	Filter	Effective wavelength	Bandpass (FWHM)	Range (km)	Resolution (km/pixel)	Sub-spacecraft		Solar phase angle
						Long	Lat	
44004.20	Clear	0.48 μ	0.20 μ	115,338	1	336°	39°	41°
44004.24	Violet	0.41 μ	0.07 μ	113,571	1	338°	38°	41°
44004.28	Green	0.55 μ	0.08 μ	111,827	1	308°	38°	41°

and albedo variations which are visible on the high resolution Voyager images of Enceladus. These images are well suited for this purpose because they represent multispectral information with better than 2-km resolution, and they were obtained at a representative range of geographical longitudes. We investigate whether a connection between the evolution of the optically active upper surface layer and underlying geologic processes exists by drawing a correlation between the ages of mapped geologic units (Smith *et al.* 1982) and surficial albedo and color. The absence of such a correlation lends credence to a model which seeks to explain the optical properties of the surface in terms of an exogenic process, such as an interaction of the satellite's surface with the E-ring, an idea which has been discussed by Buratti *et al.* (1982) and McKinnon (1983).

II. DATA SET

We searched the Voyager 2 high resolution images for sequences which fulfilled the following two requirements: good resolution of the four major mapped geologic terrains, and the availability of observations in at least the clear, violet, and orange (or green) filters. The one sequence of images which meets our criteria is listed in Table I. These images, all of which were obtained by the Voyager 2 narrow angle camera, also represent the best resolution available for Enceladus. The ideal data set for studying the scattering properties of a planet or satellite would include a representative range of solar phase angles, particularly at small angles where the body is fully illuminated. The trajectory of the Voyager spacecraft limited the images of Enceladus obtained at high resolution to solar phase angles within a few degrees of 40°.

The numerical data file for each image is an 800 × 800 array of pixels (picture elements) which contains the values of I/F for each pixel. I is the intensity of scattered sunlight and πF is the incident solar flux. For a perfect Lambert surface illuminated and viewed normally, I/F would equal unity.

Several authors (Johnson *et al.* 1983, Buratti 1984) have noted that additional color calibrations to the Voyager filters beyond those published by Danielson *et al.* (1981) are required. In general, the spectra derived from Voyager color photometry are redder than equivalent ground-based observations. Using the preliminary calibrations computed by Buratti (1984) normalized to the clear filter, we apply an additional correction factor of 0.85 to the green and orange filters. This factor brings the Voyager observation into better agreement with Earth-based measurements.

III. ALBEDO VARIATIONS

High resolution Voyager images of the surface of Enceladus suggest that its four major mapped geologic units are uniform in albedo even though they differ in age by an order of magnitude. The disk-integrated orbital light curve constructed from Voyager images has a total amplitude of less than 0.2

mag, which implies that albedo differences on the surface are less than 20% (Buratti and Veverka 1984). According to a histogram of reflectances for the surface of Enceladus, 80–90% of the surface has a reflectance at 0.48 μ between 0.90 and 1.00, with the remainder between 0.80 and 0.90 (Buratti 1984). These results contrast markedly to those of Franz and Millis (1975, 1982), who found a lightcurve amplitude of at least 0.4 mag. This discrepancy, which is discussed in more detail in Section V, is most likely due to the different geographical latitudes of the Voyager and ground-based observations.

The most prominent albedo features visible on the Voyager images are in the southern hemisphere of the trailing side, particularly in the region centered near 235° geographical long and −45° lat. These markings are barely evident on the limb of the high resolution sequences obtained by Voyager 2. They appear somewhat more clearly in the last several low resolution Voyager 1 sequences, where their morphology is reminiscent of the bright wispy streaks on the trailing sides of Rhea and Dione (see Fig. 1a). A scan of I/F values extracted along the line in Fig. 1a shows a maximum albedo change of 15% (Fig. 1b).

Of particular interest is the question of whether there exist systematic albedo and color differences among the geologic terrains. A number of quantitative tests can be performed with the Voyager images to search for systematic trends. The four accomplished in this paper are:

(1) A search for discontinuities in scans of intensity at the geologic boundaries. For the case of Ganymede, such discontinuities are distinct (Squyres and Veverka 1981). This test is a first order one and is limited by the fact that no corrections to the extracted scans are made for the lighting geometry.

(2) The fit of a scattering model to each terrain. Although this test overcomes the limitation mentioned for the first test because it corrects to an "intrinsic" albedo, it is limited by the range in incidence and emission angles obtained during the Voyager flybys of Enceladus.

(3) The comparison of points or lines which are photometrically analogous, i.e., related by Helmholtz's reciprocity principle (Minnaert 1941). If indeed the disk of Enceladus is uniform in color and albedo, any such pairs of points or lines will be identical (within the instrumental errors and other errors caused by the inexact placement of lines on the disk or shadowing by craters).

These three tests can be performed in any of the three Voyager filters (clear, violet, or green) for which the high resolution sequence was obtained in order to search for possible color differences among the terrains. A more definitive indication of such differences can be supplied by a fourth test:

(4) The construction of color ratios. In this paper two types of ratios are created; one is a green/violet line traversing all four geologic units, and the other is a green/violet map of Enceladus.

Figure 2a is the geological map prepared by the Voyager imaging team (Smith *et al.* 1982). Figure 2b shows the image obtained in the clear filter on which the map is largely based. According to crater counting statistics prepared by Plescia and Boyce (1983), the age of the oldest portions of the cratered terrain is 3.8 billion years, while the upper age limit for the smooth and ridged plains is a few hundred million years. Figure 3, a scan of I/F values along the photometric equator of the image in Fig. 2b with the interfaces between the geologic units marked, represents the results of the first test. No albedo changes are perceptible at the boundaries of the units.

The second test is a more quantitative indication of photometric differences among the terrain units and is obtained by fitting the I/F values for pixels within each geologic unit to a scattering law. Scattering models developed during the past 6 years (Hapke 1981, Lumme and Bowell 1981,

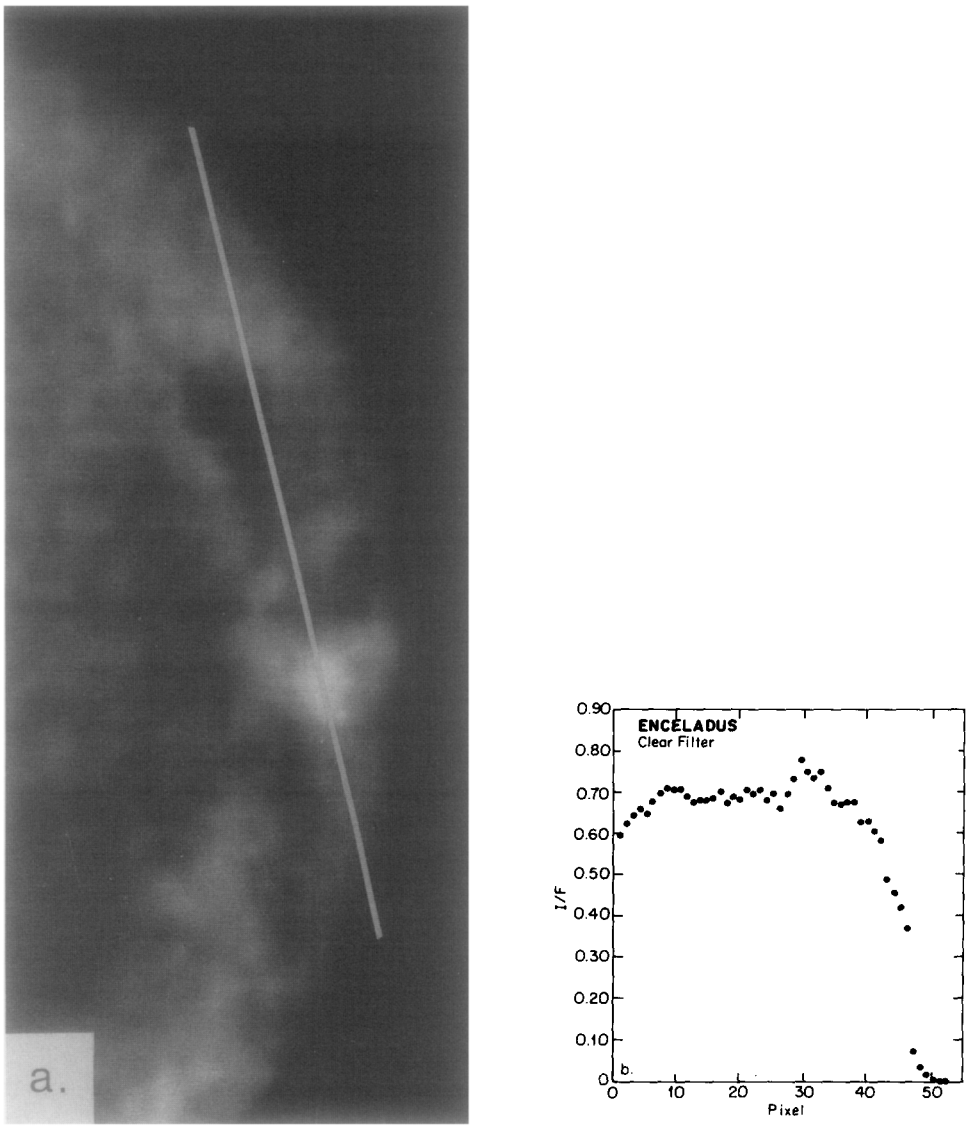

FIG. 1. (a) An enhanced version of the Voyager 1 clear filter image showing the most prominent albedo feature visible on Enceladus (FDS No. 34929.56: resolution, 13 km/pixel; phase angle, 14°; subspacecraft longitude, 252°; subspacecraft latitude, −5°). (b) A scan of I/F values extracted along the white line from (a). Albedo variations of 10–15% are evident.

Goguen 1981) are not well enough constrained to be fit over the very limited viewing geometry of the high resolution Voyager images of Enceladus. Minnaert's equation (Minnaert 1961), a simple, empirical function which depends on only two parameters, can be fit to individual terrains for the purpose of understanding their degree of uniformity. Scans of 3 × 3 pixel-averaged points were extracted from each terrain and fit to the equation

$$I = FB_0\mu_0^k\mu^{k-1}, \qquad (1)$$

where k is the limb darkening parameter, μ_0 and μ are the cosines of the incidence and emission angles, and B_0 is proportional to

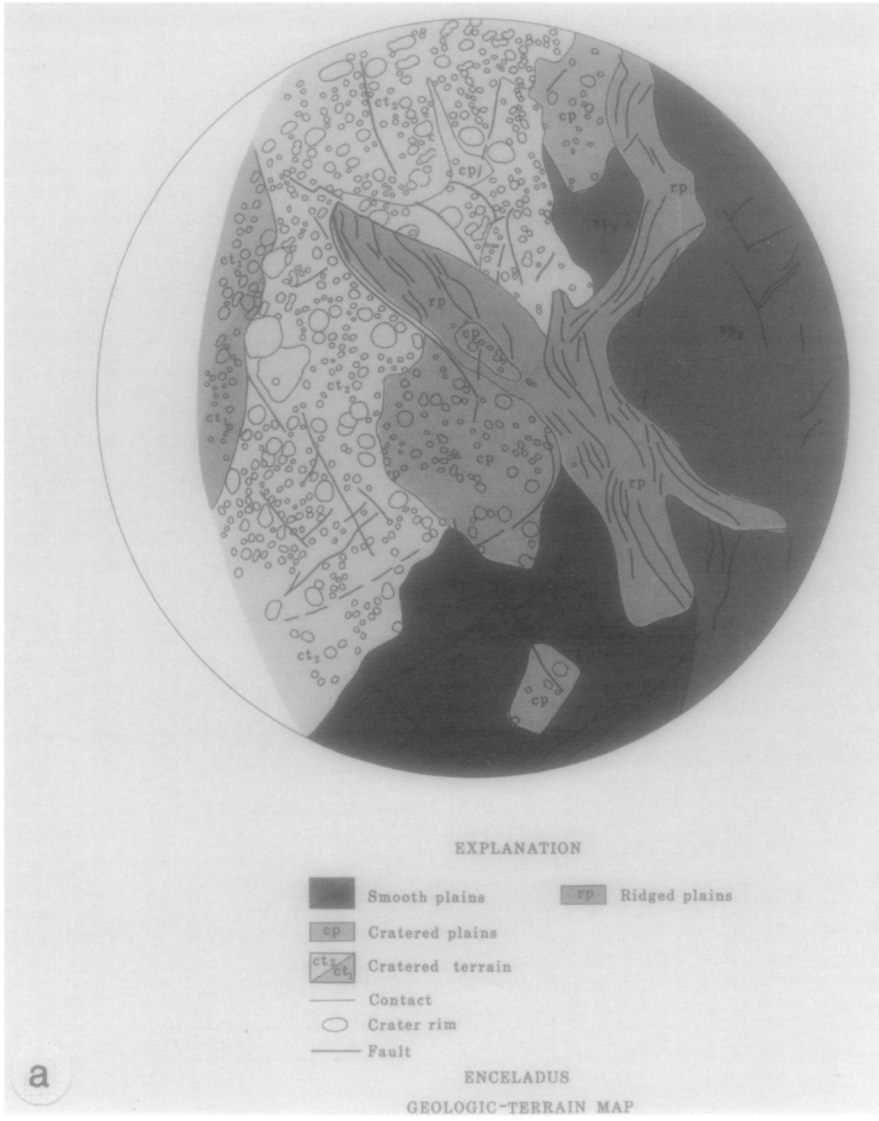

FIG. 2. The geologic map of Enceladus prepared by the Voyager imaging team (Smith *et al.* 1982, copyright 1982, American Association for the Advancement of Science). (b) The mosaic on which the map is based. It is constructed from high resolution images obtained in the clear filter. (The white line refers to Fig. 8.)

the albedo of the surface (for a phase angle of 0°, B_0 equals the normal reflectance). The nonlinear least-squares fits for B_0 and k are listed for each scan in Table II (A and $f(\alpha)$ are discussed later). Within the errors of measurements, there is no difference in the fits for each terrain. The values for k are higher than what is typical for icy satellites (Buratti and Veverka 1984) but lower than unity, the value for a perfectly diffuse (Lambert) surface dominated by multiply scattered radiation.

Goguen (1981) pointed out that a fit to Minnaert's equation for a nonzero phase angle yields different results depending on how far from the photometric equator the

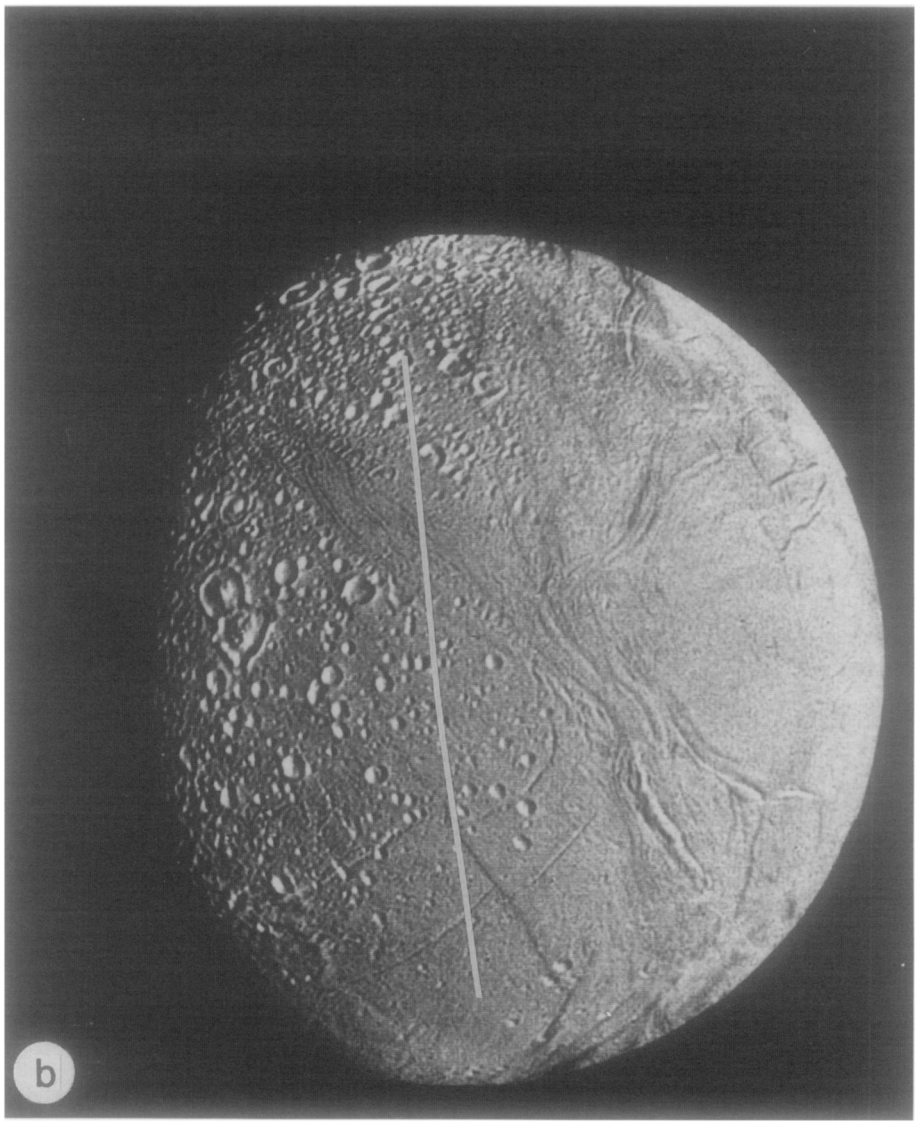

FIG. 2—*Continued.*

TABLE II

PHOTOMETRIC FUNCTION PARAMETERS (CLEAR FILTER)

Terrain	B_0	k	$f(\alpha)$	A
Smooth plains	0.82 ± 0.01	0.76 ± 0.01	1.41 ± 0.01	0.61 ± 0.02
Cratered terrain	0.84 ± 0.02	0.74 ± 0.03	1.50 ± 0.03	0.67 ± 0.07
Ridged plains	0.84 ± 0.01	0.77 ± 0.02	1.40 ± 0.02	0.52 ± 0.04
Cratered plains	0.84 ± 0.01	0.74 ± 0.02	1.48 ± 0.02	0.63 ± 0.04

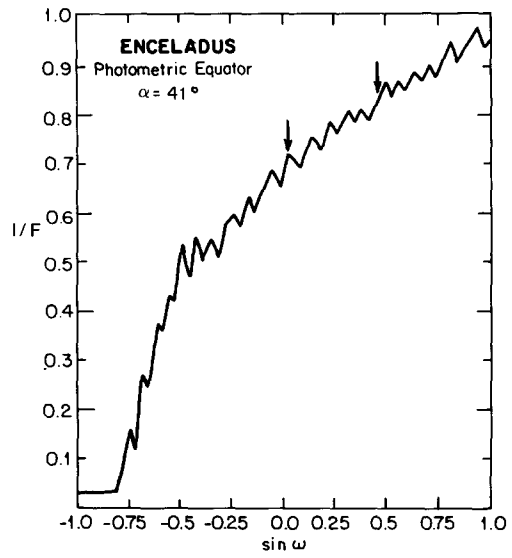

FIG. 3. A scan of I/F values extracted along the photometric equator of Fig. 2b (α is the phase angle and ω is the photometric longitude). The right arrow marks the interface between the smooth plains and ridged plains, and the left arrow marks the interface between the ridged plains and cratered terrain. No systematic albedo differences among the three terrains are evident.

measurements are obtained. He measured Minnaert's parameters for a barium sulfate sample at a phase angle of 45° and found that k changed from a value of 1.07 along the photometric equator to 1.02 at the mirror meridian, while B_0 changed from 1.03 to 0.99. For another sample with a normal reflectance of 0.69, k changed from 0.75 to 0.95 over the same range. To test whether this effect might bias our results in some way, we systematically extracted lines from the center of the satellite to the limb in 10° increments from the equator to the pole and fit the lines to Eq. (1). B_0 changed less than 3% and not consistently up or down. Except for the two lines closest to the photometric equator, k was similarly constant. Because none of the scans extracted for the fits in Table II are near the photometric equator or at photometric latitudes greater than 45°, we conclude that this effect does not bias our results beyond 1–2%.

The scans representing the four terrains can also be fit to a simple photometric function of the form (Buratti 1984)

$$I = F\{[f(\alpha)A\mu_0/(\mu + \mu_0)] + (1 - A)\mu_0\}, \quad (2)$$

where $f(\alpha)$ is the surface phase function and A is a parameter such that $A = 1$ is a lunar law (pure single scattering) and $A = 0$ is Lambert's law (diffuse scattering). The similarity in the best-fit values for A and $f(\alpha)$ (see Table II) for each of the four terrains further confirms the finding that the optical properties of the upper surface layer are uniform across the terrains.

It should be noted that the limited geographical range of the four terrains, coupled with the lack of high resolution data obtained over a range of lighting geometries, constrains our study—or any study based on Voyager images—to be based on less than a full range of radiance incidence and emission angles. Table III lists the ranges of μ and μ_0 fit for each terrain. Although there is overlap among all four terrains, the full ranges for each terrain do differ and in some cases are quite restricted. This factor may contribute to biases in the fits that are not expressed in the formal errors (see especially Table II).

A further check on the similarity in albedo between the terrain types can be demonstrated by test 3: a comparison of points which are equivalent according to the reciprocity principle (Minnaert 1941). If the surface of Enceladus is indeed uniform in albedo and scattering behavior, the I/F values of pairs of lines with photometric coordinates which are reciprocal points of each

TABLE III

RANGES IN VIEWING GEOMETRY

Terrain	Range in μ	Range in μ_0
Smooth plains	0–1.0	0.66–0.84
Cratered terrain	0.71–0.99	0.07 – 0.85
Ridged plains	0.79–0.97	0.36–0.87
Cratered plains	0.51–0.99	0–0.75

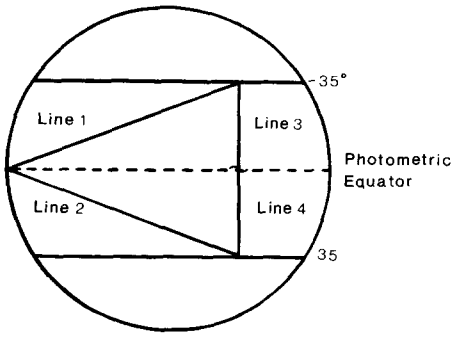

FIG. 4. Three examples of pairs of photometrically analogous lines: 1 and 2; 3 and 4; and the lines at photometric latitudes of 35° and −35°.

other should be identical. Three such pairs of lines are shown schematically in Fig. 4. Figure 5 shows the superposition of the two analogous lines for all three pairs. Except for scatter from shadows cast by large craters, the agreement between pairs of lines is very good.

There are in fact albedo markings visible over small areas on the high resolution images, particularly near geographical longitude and latitude of (315°, −20°) and (195°, 15°). It is difficult to quantify them because the shadowing by grooves and ridges causes additional albedo changes at nonzero phase angles. They may be as high as 10% and extend over 200 km^2. In any case, these changes are not correlated with the boundaries of the geological units.

In conclusion, the four major mapped geologic terrains of Enceladus, which differ in crater density and presumably age by at least an order of magnitude, have similar albedos and scattering properties over the range of viewing geometries sampled during the near encounter of the satellite.

IV. COLOR VARIATIONS

A further indication of differences in the optical properties of a planet's upper surface layer is given by color variations as a

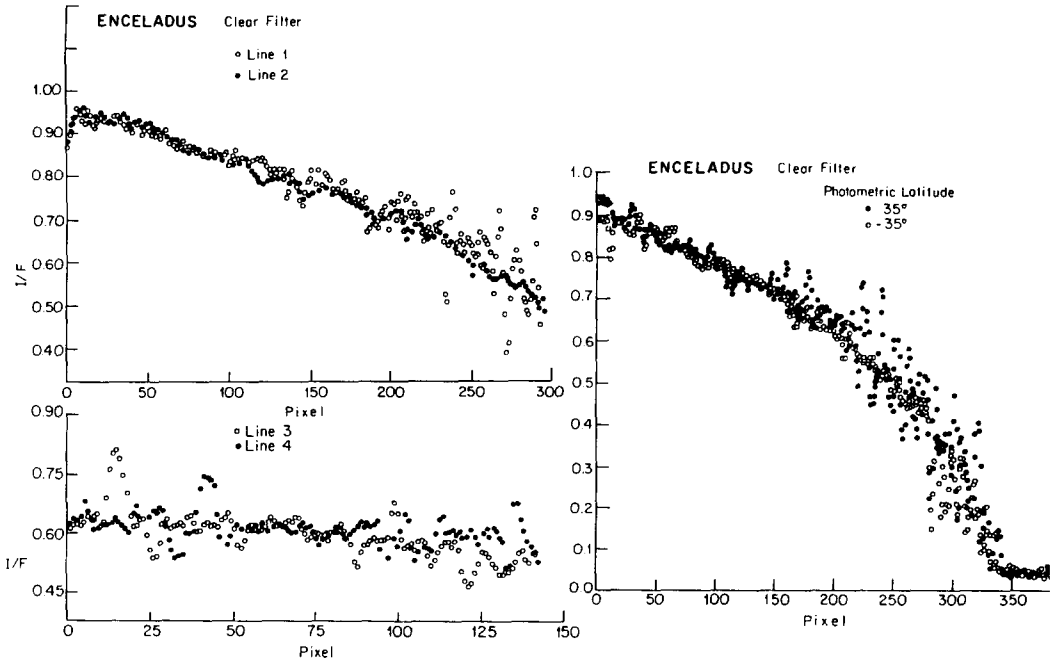

FIG. 5. *I/F* values of the three pairs of photometrically analogous lines depicted in Fig. 4 for image 44004.20 (which is essentially identical to Fig. 2b). Although there is a large amount of scatter in the data due to shadowing by craters, the average values are the same to within 2–3% (our major source of error is in positioning and registering the pairs of lines).

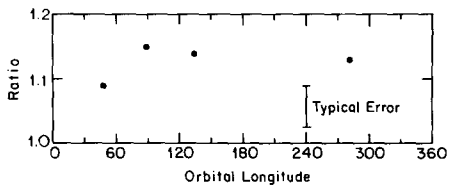

FIG. 6. The available disk-integrated orange to violet ratios as a function of subspacecraft geographical longitude. To within the error bars, there are no color changes.

function of geographic position. A rudimentary analysis of such changes is represented by an orbital lightcurve constructed from disk-integrated color ratios. The available orange/violet ratios for Enceladus are shown in Fig. 6. Within the error bars, the color ratio is approximately constant.

Another test for disk-resolved color changes involves extending the fits of a photometric scattering law (test 2) for each terrain to additional Voyager filters. The high resolution imaging sequence listed in Table I includes observations obtained with the violet and green filters (no ultraviolet or orange images were taken in this sequence). Table IV lists the results of fitting scans transversing the geologic units to Minnaert's equation using data from these two filters (we used the same scans as those for the fits listed in Table II). The uniformity in albedo is again remarkable, and there are no measurable differences in the limb darkening parameters of the four terrains in either filter. Tables II and IV also show that there is little if any color dependence to the limb darkening parameter.

The third test consists of comparing the photometrically reciprocal lines (Fig. 3) in the green and violet filters. Our results are the same as those for the clear filter: none of the pairs of lines show a difference in albedo or shape. An example of one pair of lines for the violet filter is shown in Fig. 7.

The uniformity in albedo for the geologic units in all three filters implies that there are no color changes as a function of position on the portion of the disk imaged by Voyager. This result can be further studied by test 4, which is to compute a ratio of identical scans, extracted from the violet and green filters, which traverse all four geologic units. The resulting ratio, which was constructed from scans extracted along the white line in Fig. 2b, is shown in Fig. 8. Even though there is still a noise level of approximately 5% (due primarily to shadowing by topography and inexact registration between the two images), the average value of the ratio is constant for all four terrains.

The final test for color changes across the disk of Enceladus consists of constructing a global ratio of two color images of the satellite. We stored the I/F values for the green and violet images in two different channels of a Grinnell image display device and wrote the ratio of the two images into a third channel. We then ran a contour routine on the resulting image to see if any distinct contours, which would indicate sys-

TABLE IV

MINNAERT PARAMETERS FOR GREEN AND VIOLET FILTERS

Terrain	Green		Violet	
	B_0	k	B_0	k
Smooth plains	0.85 ± 0.01	0.73 ± 0.01	0.80 ± 0.01	0.75 ± 0.02
Cratered terrain	0.86 ± 0.02	0.73 ± 0.01	0.82 ± 0.01	0.71 ± 0.03
Ridged plains	0.85 ± 0.01	0.72 ± 0.01	0.81 ± 0.01	0.74 ± 0.02
Cratered plains	0.88 ± 0.02	0.72 ± 0.02	0.80 ± 0.01	0.73 ± 0.02

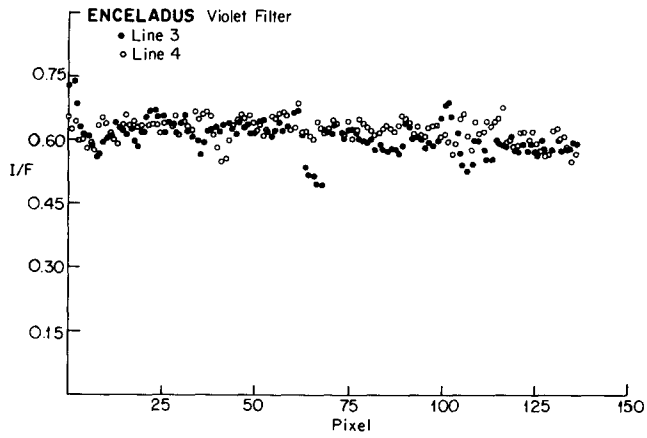

FIG. 7. An example of a pair of photometrically analogous lines (lines 3 and 4 from Fig. 4) for the violet filter (FDS image No. 44004.24).

tematic color changes, appeared. No contours appeared down to the level of 25 equally spaced bins of the ratioed I/F values, which corresponds to a 5% change in the color ratio.

V. CONCLUSIONS AND DISCUSSIONS

Although albedo variations of 10–15% do occur over areas of the surface of Enceladus observed by the two Voyager spacecraft, the high resolution images acquired by Voyager 2 show uniform albedos and colors for the four major mapped geological terrains. In the clear, green, and violet filters, the terrains follow similar scattering laws over the range of lighting geometries listed in Table III, and average albedos for each color differ by only 1–2%. No color changes above the noise level were detected in either disk-integrated or disk-resolved measurements.

Both ground-based (Franz and Millis

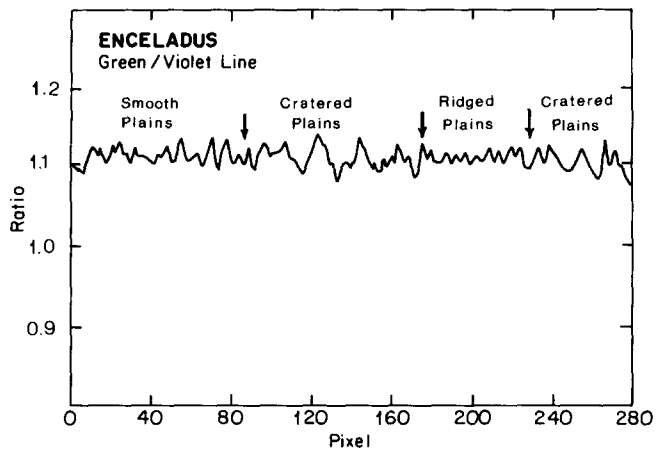

FIG. 8. A line representing the ratio of green and violet I/F values extracted along the white line in Fig. 2b. The interfaces between the terrains are marked by arrows. Although there is ~5% scatter in the data (caused mainly by imperfect registration between crater shadows), the average ratio for the three terrains is the same to within 2–3%.

1975) and Voyager lightcurves (Buratti and Veverka 1984) show that the trailing side of Enceladus is brighter than the leading side. The separately computed phase coefficients between 13° and 43° in the Voyager clear filter are 0.015 ± 0.002 (trailing side) and 0.021 ± 0.002 (leading side) mag/degree. The lower phase coefficient is expected for the brighter trailing hemisphere because the increased importance of multiple scattering reduces the effect of mutual shadowing among regolith particles. One might expect that the higher albedo of the trailing side is due to the concentration of geologically more recent terrain there. In the absence of high resolution imaging observations for the leading side, we cannot preclude this possibility. However, since geologic units differing in age by more than an order of magnitude on the trailing side have nearly identical albedos, we believe it is unlikely that the explanation is this simple. Perhaps the very bright markings barely seen in the images cover extensive portions of the Southern hemisphere of the trailing side not included in the high resolution coverage. Another piece of supporting evidence for this latter idea is that accurate ground-based photometric observations of Enceladus obtained by Franz and Millis from 1973 to 1980 (Franz and Millis 1982) show an amplitude in the rotational lightcurve of 0.4 mag (i.e., at least twice the Voyager amplitude), with the maximum at 270°. Whereas the high resolution Voyager images (Table I) were obtained at high northern subspacecraft latitudes and include no information south of −30° lat, Earth-based observations include the entire Southern hemisphere. The discrepancy between the Voyager and telescopic observations could possibly be reconciled by having virtually the entire Southern hemisphere covered by a material 20% brighter than the northern hemisphere. The bright albedo features visible in the low resolution Voyager 1 images (Fig. 1) are in fact located at the edge of the southern region.

Two other speculative possibilities are that the brightness variations on Enceladus are transient or that optical effects in the E-ring such as a larger optical depth at elongation cause Enceladus to be brighter at eastern elongation. The latter is unlikely because of the tenuousness of the ring.

Enceladus' unusually high geometric albedo implies that there is less opaque material in the surface layer than on other icy bodies in the Solar System. Measurements by Clark (1981) showed that a fractional coverage of montmorillonite grains on frost of only 0.002 ± 0.001 caused a drop from 0.98 to 0.90 in the reflection spectrum at 0.65 μ. Since 0.90 is already less than the reflectivity of Enceladus at 0.59 μ, the fraction of opaques is probably even less than this amount. However, a recent rediscussion of Clark's results by Spencer (1987) suggests a higher opaque content is possible.

Another supporting observation for the extremely low fraction of opaque material on the surface of Enceladus is the flatness of its spectrum into the UV (Buratti 1984). For the icy Saturnian and Galilean satellites, there is an inverse correlation of the slope of the spectrum between 0.34 and 0.60 μ and the geometric albedo (Millis and Thompson 1975, Johnson *et al.* 1983, Buratti 1984). A simple explanation for this phenomenon is provided by modeling the surfaces of these icy satellites as mixtures of bright, spectrally flat ice and darker, red contaminants. Because Enceladus has both the highest geometric albedo and the smallest slope, it follows that it has the lowest fraction of opaque contaminants of these satellites.

It is unlikely that the photometric uniformity of Enceladus is due to a primordial, intrinsic compositional homogeneity. The bulk density of Enceladus is 1.2. It is difficult to imagine a mechanism which could have so perfectly fractionated the heavier, lower albedo siliceous material below the optically active regolith. In addition, the 4-billion-year-old cratered terrain would have been subjected to the usual darkening by

micrometeoritic bombardment and, possibly, radiation.

The lack of correlation of spectrophotometric properties with the local geologic age (as determined by crater counts) and the high geometric albedo of Enceladus suggest that its optical properties are not determined by underlying geologic processes, but by a relatively recent ubiquitous surface layer. Infall of material from the E-ring is the most likely source of this layer.

The E-ring itself is probably the result of active surface processes on Enceladus. The four basic models that have been proposed for its origin are

(1) micrometeorite impact and subsequent escape of surface particles (Smoluchowski and Torbett 1982);

(2) a single impact and ejection of particles by a larger, 20-km-sized body (McKinnon 1983);

(3) volcanic ejection of particles from Enceladus (Terrile and Cook 1981, which is actually a combination of impact and volcanism; Pang *et al.* 1984); and

(4) emplacement of water–ammonia volcanic flows on Enceladus (Herkenhoff and Stevenson 1984). In the latter case, tidal heating is necessary; it has been shown to be marginally possible (Squyres *et al.* 1983, Lissauer *et al.* 1984).

We believe the high reflectivity of the particles that are accreted onto Enceladus is strong evidence for placing their source originally on Enceladus; visual single particle albedos for the other rings in the Saturnian System range from 0.20 to 0.60 (Esposito *et al.* 1984). (Of course, the other piece of compelling evidence is that the maximum thickness of the E-ring coincides with the orbit of Enceladus (Baum *et al.* 1981).) More specifically, the high albedo suggests they are the result of a geologic process that produces fresh ice; the products of impacts would not be expected to have an albedo which is 25% higher than any other object in the Saturnian system. Because the destruction mechanisms of sputtering and plasma drag determine a lifetime of about 10,000 years for typical particles in the E-ring (Morfill *et al.* 1983), there is probably an active influx of material into the E-ring if it is more than a short-lived phenomenon.

Hartmann (1980) noticed an inverse correlation between crater density (and presumably age) and albedo for the Galilean satellites. He attributed the cause of this correlation to a mechanism in which impacts darken the surface by vaporizing the icy component. The lack of a similar correlation for the surface of Enceladus may indicate that infall from the E-ring dominates any gardening caused by meteoritic impacts.

There is photometric evidence that the structure of the regolith resulting from the reaccretion of E-ring particles is similar to that produced by micrometeoritic gardening. The solar phase curves and disk-resolved scattering properties of icy satellites look more Lambertian as their geometric albedo increases. This observation can be explained by the increased importance of multiple scattering, which provides a diffuse Lambert-like component to the scattering function. Fits of photometric observations to a radiative transfer model which depends on the regolith porosity, single particle phase function, single scattering albedo, and macroscopic roughness show that both the disk-integrated and disk-resolved scattering properties of Enceladus are best reproduced by a high single scattering albedo (0.99) and more lunar-like values for the parameters which define the structure of the regolith (Buratti 1985).

Using our disk-resolved observations only (Buratti and Veverka 1984), Pang *et al.* (1985) have invoked the existence of "micron-size ice spheres" on Enceladus' surface. Specifically, they note that our finding that the linear coefficient of a second order polynomial fit to Enceladus' phase curve is negative gives evidence for their claim. We find no justification for drawing this connection; the negative coefficient in the linear term is simply a result of the larger Lambert component in Enceladus' scattering function, which in turn is due to its high single scattering albedo and concomitant

high degree of multiple scattering (Buratti 1985). In any case, more telescopic observations at solar phase angles below 6° are required to understand the surface of Enceladus. It is at these low phase angles that the phase curve is most diagnostic of the porosity of the regolith (Irvine 1966, Hapke 1981).

It can be legitimately asked why Enceladus is not a pure Lambert scatterer, since laboratory measurements of surfaces with a geometric albedo of unity are nearly Lambertian (Oetking 1966, Goguen 1981). Recent experiments have shown that excavating a crater into a Lambert surface causes the scattering to become markedly non-Lambertian (Buratti and Veverka 1985). For Enceladus, other contributing factors are mutual shadowing among regolith particles and a nonisotropic single particle phase function. With the only measurements of the photometric and phase functions of ice and snow being terrestrial field measurements obtained in the 1950s (see Veverka 1973), we cannot quantify the latter two factors.

Similarly, it is difficult to quantify by photometric analysis the degree of macroscopic roughness on Enceladus, since there is an absence of Voyager coverage at phase angles larger than 43°, where the photometric effects of roughness become significant (Hapke 1984, Buratti and Veverka 1985). The observations at 41° are consistent with a mean slope angle for rough features of 30° (Buratti 1985), which is similar to values for the Moon and Mimas, but larger than those for Europa and Mercury (Buratti 1985, Hapke 1977).

ACKNOWLEDGMENTS

This work represents one phase of research carried out at the Jet Propulsion Laboratory, California Institute of Technology, under contract with NASA. I thank J. Goguen and E. Bowell for careful reviews.

REFERENCES

BAUM, W. A., T. KREIDL, J. A. WESTPHAL, G. E. DANIELSON, P. K. SEIDELMANN, D. PASCU, AND D. G. CURRIE 1981. Saturn's E-ring, I, CCD observations of March 1980. *Icarus* **47,** 84–96.

BURATTI, B. 1984. Voyager disk resolved photometry of the Saturnian satellites. *Icarus* **59,** 392–405.

BURATTI, B. 1985. Application of a radiative transfer model to bright icy surfaces. *Icarus* **61,** 208–217.

BURATTI, B., AND J. VEVERKA 1984. Voyager photometry of Rhea, Dione, Tethys, Enceladus and Mimas. *Icarus* **58,** 254–264.

BURATTI, B., AND J. VEVERKA 1985. Photometry of rough planetary surfaces: The role of multiple scattering. *Icarus* **64,** 320–328.

BURATTI, B., J. VEVERKA, AND P. THOMAS 1982. Enceladus: Implications of its unusual photometric properties. *Bull. Amer. Astron. Soc.* **14,** 737–738.

CLARK, R. N. 1981. Water frost and ice: The near-infrared spectral reflectance 0.65–2.5 μ. *J. Geophys. Res.* **86,** 3087–3096.

CRUIKSHANK, D. P. 1979. Physical properties of the satellites of Saturn. *Rev. Geophys. Space Phys.* **17,** 165–176.

DANIELSON, G. E., P. KUPFERMAN, T. JOHNSON, AND L. SODERBLOM 1981. Radiometric performance of the Voyager cameras. *J. Geophys. Res.* **86,** 8683–8689.

ESPOSITO, L. W., J. N. CUZZI, J. B. HOLBERG, E. A. MAROUF, G. L. TYLER, AND C. C. PORCO 1984. Saturn's rings: Structure, dynamics, and particle properties. In *Saturn* (T. Gehrels and M. S. Matthews, Eds.). Univ. of Arizona Press, Tucson.

FRANZ, O. G., AND R. L. MILLIS 1975. Photometry of Dione, Tethys, and Enceladus on the UBV system. *Icarus* **24,** 433–442.

FRANZ, O. G., AND R. L. MILLIS 1982. Orbital brightness variations and geometric albedos of Mimas, Enceladus, Tethys, Dione, and Rhea. In *Saturn: Programs and Abstracts from Meeting,* p. 74. May 1982, Tucson.

GOGUEN, J. D. 1981. *A Theoretical and Experimental Investigation of the Photometric Functions of Particulate Surfaces.* Ph.D. thesis, Cornell University.

HAPKE, B. W. 1977. Interpretations of optical observations of Mercury and the Moon. *Phys. Earth Planet. Inter.* **15,** 264–274.

HAPKE, B. W. 1981. Bidirectional reflectance spectroscopy. I. Theory. *J. Geophys. Res.* **86,** 3039–3054.

HAPKE, B. W. 1984. Bidirectional reflectance spectroscopy. III. Correction for macroscopic roughness. *Icarus* **59,** 41–59.

HARTMANN, W. K. 1980. Surface evolution of two component stone/ice bodies in the Jupiter region. *Icarus* **44,** 441–453.

HERKENHOFF, K. E., AND D. J. STEVENSON 1984. Formation of Saturn's E-ring by evaporation of liquid from the surface of Enceladus. *Lunar Planet. Sci.* **15,** 361–362.

IRVINE, W. M. 1966. The shadowing effect in diffuse reflection. *J. Geophys. Res.* **71,** 2931–2937.

JOHNSON, T. V., L. A. SODERBLOM, J. A. MOSHER, G. E. DANIELSON, A. F. COOK, AND P. KUPFERMAN

1983. Global multispectral mosaics of the icy Galilean satellites. *J. Geophys. Res.* **88,** 5789–5805.

LISSAUER, J. J., S. J. PEALE, AND J. N. CUZZI 1984. Ring torque on Janus and the melting of Enceladus. *Icarus* **58,** 159–168.

LUMME, K., AND BOWELL, E. 1981. Radiative transfer in the surfaces of atmosphereless bodies. I. Theory. *Astron. J.* **86,** 1694–1704.

MCKINNON, W. B. 1983. Origin of the E-ring: Condensation of impact vapor or boiling of impact melt? *Lunar Planet. Sci.* **14,** 487–488.

MILLIS, R. L., AND D. T. THOMPSON 1975. UBV photometry of the Galilean satellites. *Icarus* **26,** 408–419.

MINNAERT, M. 1941. The reciprocity principle in lunar photometry. *Astrophys. J.* **93,** 403–410.

MINNAERT, M. 1961. Photometry of the Moon. In *The Solar System. III. Planets and Satellites* (G. P. Kuiper and B. M. Middlehurst, Eds.). Univ. of Chicago Press, Chicago.

MORFILL, G. E., E. GRUN, AND T. V. JOHNSON 1983. Saturn's E, G, and F rings: Modulated by the plasma sheet? *J. Geophys. Res.* **88,** 5573–5579.

NOLAND, M., J. VEVERKA, D. MORRISON, D. P. CRUIKSHANK, A. R. LAZAREWICZ, N. D. MORRISON, J. L. ELLIOT, J. GOGUEN, AND J. A. BURNS 1974. Six-color photometry of Iapetus, Titan, Rhea, Dione, and Tethys. *Icarus* **23,** 334–354.

OETKING, P. 1966. Photometric studies of diffusely reflecting surfaces with applications to the brightness of the Moon. *J. Geophys. Res.* **71,** 2505–2513.

PANG, K. D., J. LUNINE, AND J. W. RHOADS 1985. The unusual photometric properties of some outer satellites: evidence for geologic activity? *Lunar Planet. Sci.* **16,** 649–650.

PANG, K. D., C. C. VOGE, J. W. RHOADS, AND J. M. AJELLO 1984. The E-ring of Saturn and satellite Enceladus. *J. Geophys. Res.* **89,** 9459–9470.

PLESCIA, J. B., AND J. M. BOYCE 1983. Crater numbers and geological histories of Iapetus, Enceladus, Tethys, and Hyperion. *Nature* **301,** 666–670.

SMITH, B., L. SODERBLOM, R. BATSON, P. BRIDGES, J. INGE, H. MASURSKY, E. SHOEMAKER, R. BEEBE, J. BOYCE, G. BRIGGS, A. BUNKER, S. COLLINS, C. HANSEN, T. JOHNSON, J. MITCHELL, R. TERRILE, A. COOK, J. CUZZI, J. POLLACK, G. DANIELSON, A. INGERSOLL, M. DAVIES, G. HUNT, D. MORRISON, T. OWEN, C. SAGAN, J. VEVERKA, R. STROM, AND V. SUOMI 1982. A new look at the Saturn system. *Science* **215,** 504–536.

SMOLUCHOWSKI, R., AND M. TORBETT 1982. The E-ring of Saturn (abstract). In *Proceedings of the Planetary Rings/Anneaux des Planetes Conference,* Toulouse, France, August 1982.

SPENCER, J. R. 1987. Icy Galilean satellite reflectance spectra: Less ice on Ganymede and Callisto? *Icarus* **70,** 99–110.

SQUYRES, S. W., R. T. REYNOLDS, P. M. CASSEN, AND S. J. PEALE 1983. The evolution of Enceladus. *Icarus* **53,** 319–331.

SQUYRES, S. W., AND J. VEVERKA 1981. Voyager photometry of surface features on Ganymede and Callisto. *Icarus* **46,** 137–155.

TERRILE, R. J., AND A. F. COOK 1981. Enceladus: Evolution and possible relationship with Saturn's E-ring. *Lunar Planet. Sci. (Suppl. A)* **12,** 10.

VEVERKA, J. 1973. The photometric properties of snow and of snow-covered planets. *Icarus* **20,** 304–310.